JOURNAL OF GEOPHYSICAL RESEARCH, VOL. 106, NO. A8, PAGES 15,415–15,428, AUGUST 1, 2001

Statistical study of auroral spirals

N. Partamies

Finnish Meteorological Institute, Geophysical Research, Helsinki, Finland

Department of Physics, University of Helsinki, Helsinki, Finland

K. Kauristie and T. I. Pulkkinen

Finnish Meteorological Institute, Geophysical Research, Helsinki, Finland

M. Brittnacher

Geophysics Program, University of Washington, Seattle, Washington

Abstract. We present results of a statistical study of 189 auroral spiral forms. The data set was collected by a systematic examination of the images recorded at five all-sky camera (ASC) stations in northern Fennoscandia and Svalbard during the winters 1996–1997 and 1997–1998. For every spiral we defined the time of occurrence, diameter, direction of motion, and distance between the adjacent spirals (wavelength) in cases of spiral streets. The magnetic activity level was determined by using the magnetic north component (B_x) recorded at the ASC station and the local auroral electrojet index (*IL* index) computed by using the data from the IMAGE magnetometer network. The typical values of the diameter, wavelength, and ratio between diameter and wavelength were 25–75 km, 125–175 km, and 2–6, respectively. According to our ASC data set, spirals are more common in the magnetic postmidnight sector than previous satellite observations suggest. Spirals drift predominantly in the same direction as the large-scale ionospheric convection. Our observations of the average drift speed of spirals of 4 km/s are comparable to the corresponding values of other auroral small-scale structures. Statistical analysis revealed that spirals occur most frequently under magnetically quiet (*IL* > -200 nT) conditions, and thus they cannot always be considered as precursors of substorm activity.

1. Introduction

Small-scale auroral arc distortions have been photographed and their generation mechanisms have been discussed since the early 1950s. In 1970, *Davis and Hallinan* [1970] categorized the fine structures in three different groups according to their size, lifetime, rotational sense, and reversibility. These groups were named folds, curls, and spirals. Spirals are the largest auroral vortices (diameters typically of 20–1300 km). They are reversible and their sense of rotation is counterclockwise when viewed from above in the Northern Hemisphere. Spirals tend to appear within both arcs and arc systems.

Davis and Hallinan [1976] made observations of spirals by using images from the Defense Meteorological Satellite Program (DMSP) satellite and all-sky cameras (ASC). Their data set showed that spirals are relatively common auroral structures, visible in more than 30% of the DMSP images. According to their study, spirals frequently occur on the nightside of the auroral oval (1800–0300 MLT). Spirals can also form a street of two or more spirals with a typical separation between the adjacent spirals (wavelength) of $\lambda \approx 100$ km [*Trondsen and Cogger*, 1998]. The spirals in the street usually have similar configuration and size, but they may also grow monotonically along the arc [*Davis and Hallinan*, 1976].

In the data set of *Davis and Hallinan* [1976], the spirals form two different subgroups in the morning sector of the oval between 0400 and 0800 MLT. The spirals in the first subgroup are relatively small and occur during magnetically active conditions. They are highly transient features with lifetimes of the order of 1 min. The rotation of these spirals seems to be reversible; i.e., they are able to both wind and unwind. The spirals of the second subgroup occur at the poleward boundary of the underlying oval. They are relatively stable, but their reversibility has not been confirmed yet. In general, in both the DMSP satellite data and the ASC data set of *Davis and Hallinan* [1976], the number of spirals is

Paper number 2000JA900172.
0148-0227/01/2000JA900172$09.00

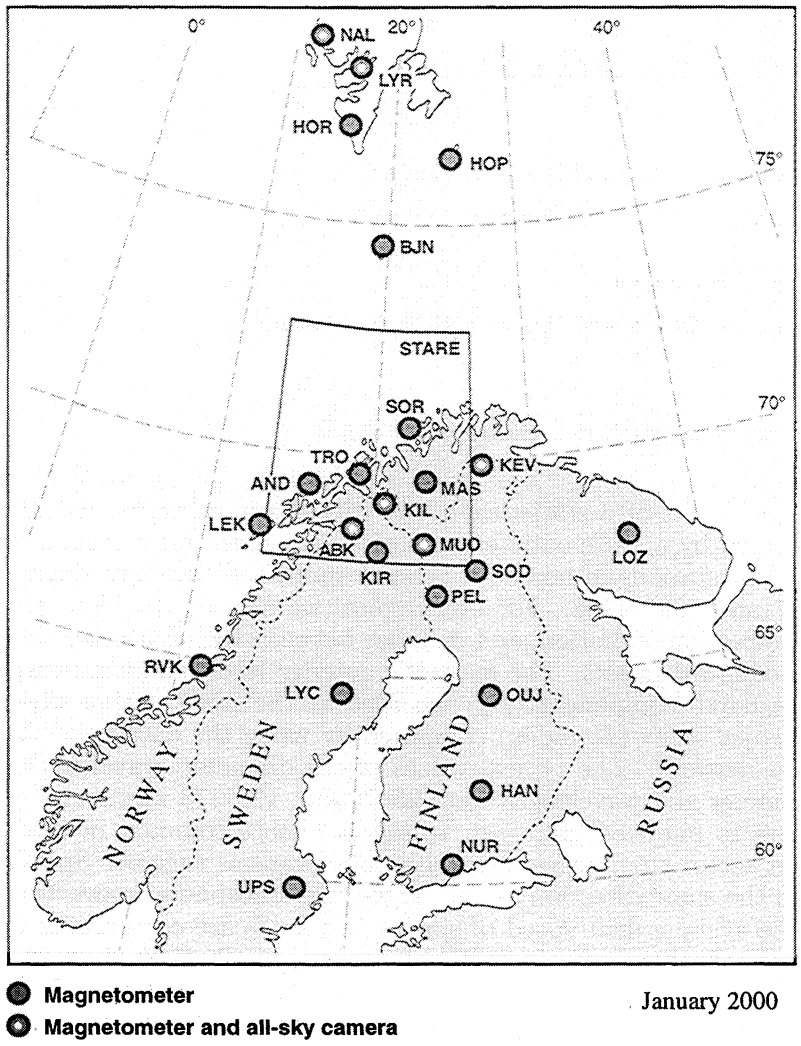

Figure 1. Map of the MIRACLE stations.

considerably smaller in the morning sector than in the evening sector.

Two examples of Polar UV images of our spirals are shown in Plates 1 and 2. In Plate 1, a street of four spirals is located at the poleward edge of the oval (top panel). The simultaneous all-sky camera images (bottom panel) are taken at the station in Longyearbyen on Svalbard. The sampling rate of the ASC is 20 s. In the UVI image, spirals resemble very much azimuthally spaced auroral forms (AAF) [*Elphinstone et al.*, 1996]. In Plate 2, a spiral (or a spiral street) locates within the main oval. The Polar image is taken about 20 s before the spiral was completely wound (last image on the right-hand side in the bottom panel), and thus the structure is not clearly visible in the UVI image. Simultaneous ASC images (bottom panel) from Kilpisjärvi show the evolution of one of the spirals and its drifting to the center of the field of view. Like the examples above demonstrate, satellite images show nicely the global context of the spirals, but ASC data are more useful when monitoring their evolution and detailed structure.

In this paper we first describe our ASC and magnetic field observations in section 2. In section 3 we present the statistical results, and we compare them with previous studies in section 4. Concluding remarks are given in section 5.

2. Description of the Data Set

2.1. MIRACLE Network

This study is based on the auroral images recorded at the five all-sky camera stations (see Figure 1) of the MIRACLE network [*Syrjäsuo et al.*, 1998] during the winters 1996–1997 and 1997–1998. This observing period contains about 16,000 hours of operation time and about 2.7 million images from ASC stations in Kilpisjärvi (KIL), Muonio (MUO), and Kevo (KEV) in Finland; Abisko (ABK) and Kiruna (KIR) in Sweden; and Longyearbyen (LYR) on Svalbard. Although KIR is not a permanent MIRACLE station, the data recorded there during one-week prototype testing (54 hours of operation time) are also included in our data set.

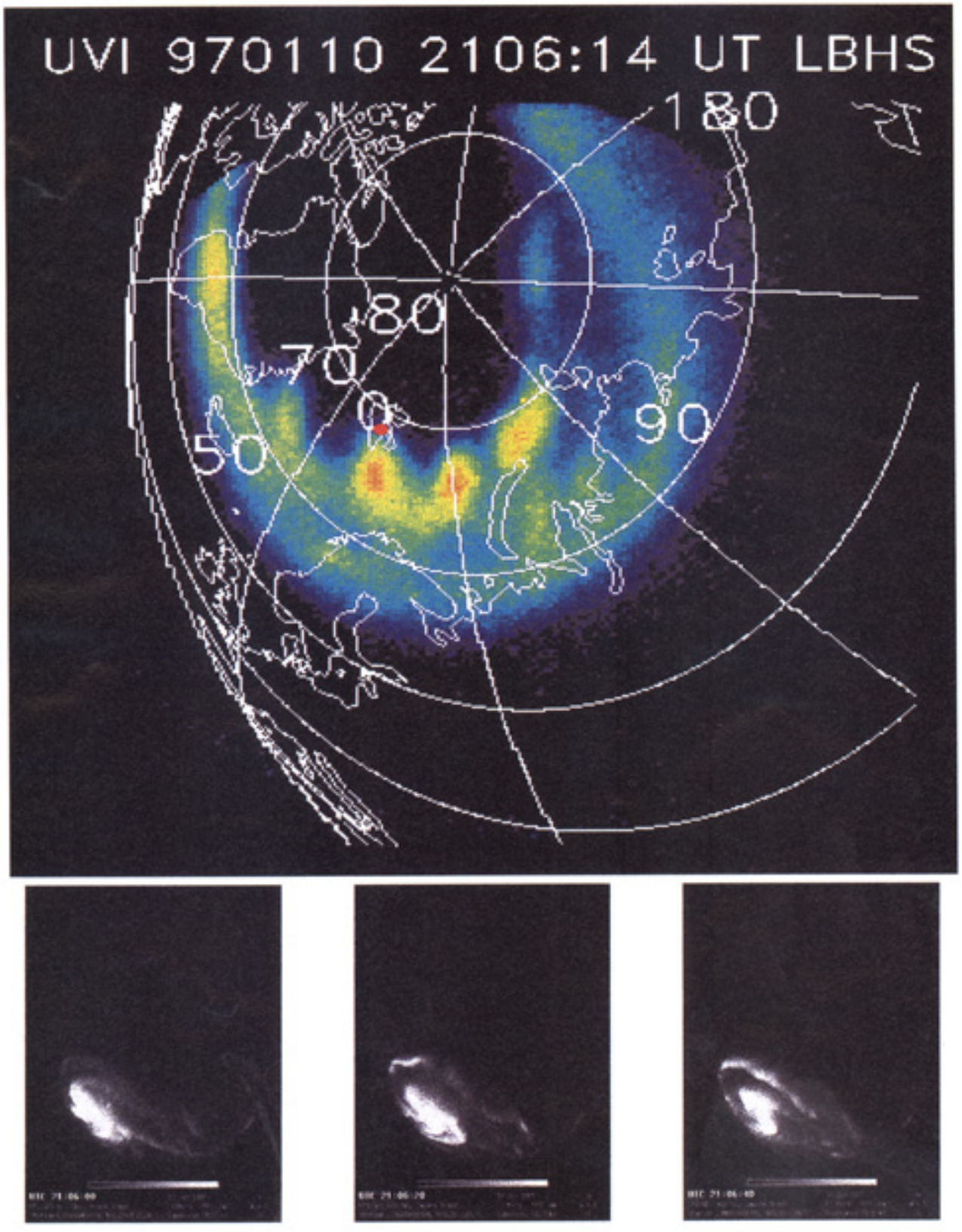

Plate 1. (top) A spiral street at the poleward edge of the oval in a Polar UVI image together with (bottom) simultaneous ASC images from Longyearbyen. The red spot in the UVI image shows the location of the Longyearbyen station on Svalbard.

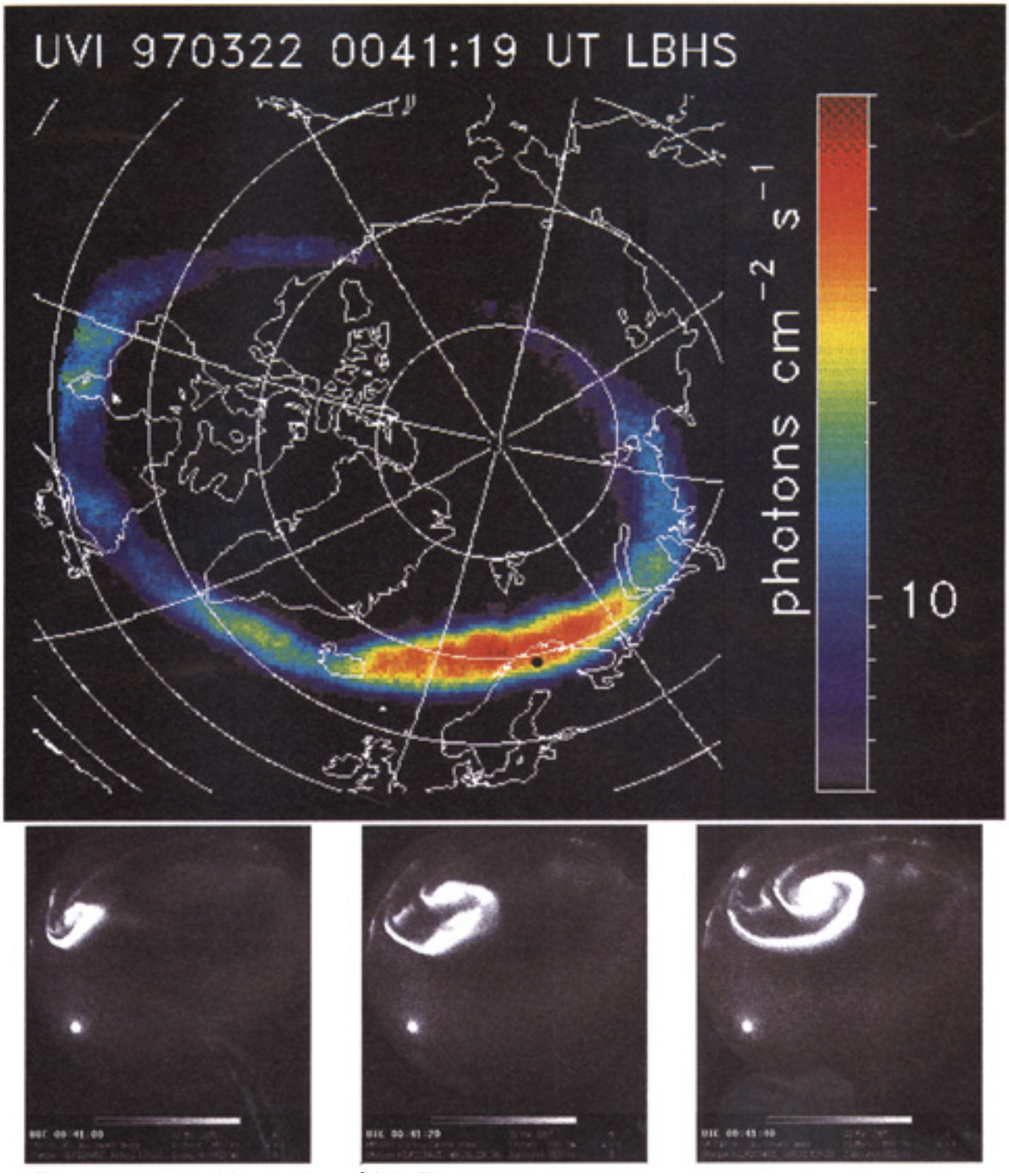

Plate 2. (top) Another spiral street at the center of the oval in a Polar UVI image and (bottom) simultaneous ASC images from Kilpisjärvi. The location of the Kilpisjärvi station in the UVI image is marked with a black spot.

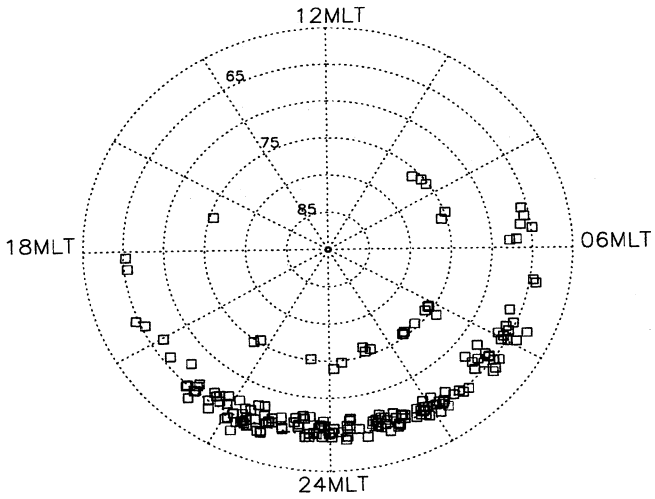

Figure 2. Distribution of spiral observations in MLT and corrected geomagnetic latitude. Squares show the locations of the center of completely wound spirals.

An ASC image covers a circular area with a diameter of about 600 km at an altitude of 110 km (with a field of view of 140° corresponding to 440 pixels in the image). The spatial resolution of an ASC image depends on the elevation angle: it is much lower near the horizon than at zenith. On average the resolution is roughly 600 km/440 pixels = 1.4 km/pixel. In case of bright auroras, blooming of the charges in the camera can somewhat reduce the resolution, which still is better than 10 km/pixel. The ASC images are flipped in the east-west direction, so that the motion, winding, and tilting of the auroral forms have the same direction as viewed from satellites. The time resolution of the ASC images is 20 s throughout the observation period.

The magnetometer network IMAGE includes 24 magnetometers which cover geographic latitudes from 59.90° to 78.92° (Figure 1). In this study, we used the *IL* index (local *AL* index) to characterize the strength of geomagnetic disturbances in the Scandinavian sector and ΔB_x (magnetic north component) recorded at each ASC station to study the immediate activity related to the spirals. The *IL* index is defined as the lower envelope of the $\Delta B_x(t)$ curves ($\Delta B_x(t) = B_x(t) - B_{x0}$, where B_{x0} is the daily average of $B_x(t)$) recorded at the IMAGE stations.

2.2. Selection Criteria and Parameters

A spiral winds counterclockwise when viewed from above in the Northern Hemisphere [*Davis and Hallinan,* 1976]. When looking for the spiral events, we required the rotation of the structure of at least 180° to exclude folds, kinks, and most of westward traveling surges and omega bands [*Davis and Hallinan,* 1970; *Trondsen and Cogger,* 1998]. Sometimes spirals appear in the ASC images only as bright spots within an auroral arc. In these cases, the sense of rotation of the structures was determined on the basis of the threads connecting the spot to the underlying arc or to the next spiral.

Our data set consists of 189 spiral events. The parameters determined for every spiral are the time of occurrence (UT), diameter, direction of motion, local ΔB_x, *IL* index, and location in MLT. In case of spiral streets the separation between the adjacent spirals (wavelength λ) was also measured.

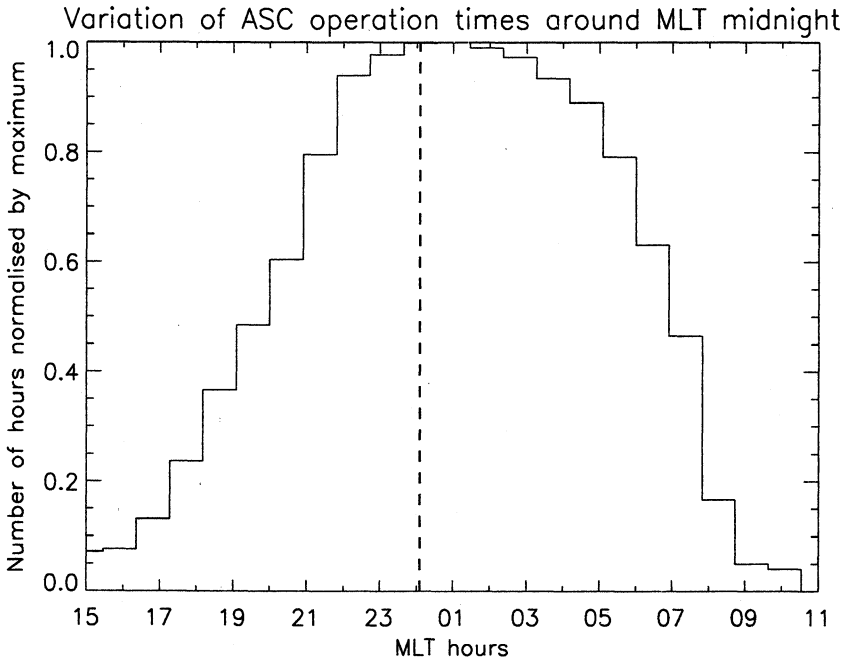

Figure 3. MLT distribution of the ASC operation hours (all ASCs) during winter 1996–1997 and 1997–1998. The histogram is normalized by the maximum number of occurrences (1284) of the midnight bin, 2400–0100 MLT. The vertical dashed line marks local magnetic midnight.

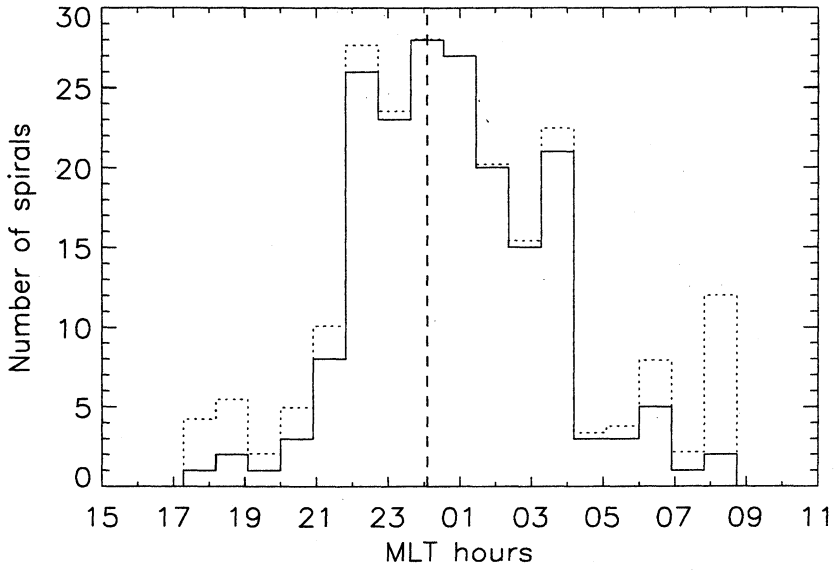

Figure 4. Distribution of the spiral observations in MLT (solid line) divided by the relative operation time of the ASCs from Figure 3 (dotted line). The difference is surprisingly small.

The MLT was estimated by assuming that Muonio is at magnetic midnight (MLT = 2400) at about 2130 UT (i.e., at MUO MLT = UT + 2.5 hours). Furthermore, 1 MLT hour roughly corresponds to 15° in geographic longitude, which was used to compute the MLTs at the other stations.

3. Statistical Results

3.1. MLT Distribution

Figure 2 represents the distribution of the spiral locations at the observation time in corrected geomagnetic (CGM) latitude and magnetic local time. The gap around 70° latitude is due to the Arctic Sea; i.e., it separates the observations of the four mainland stations and those of LYR. The few dayside events at high latitudes in the noon sector were observed at LYR on Svalbard. Most of the spiral events took place in the midnight sector. There is a clear difference between the number of occurrences before and after midnight with more observations in the morning sector. This disagrees with the results by *Davis and Hallinan* [1976], who found more spirals in the evening sector (see their Figure 7).

The MLT distribution of our spiral observations is affected by variations in the coverage of the ASC recordings and cloudiness at the stations. Figure 3 shows that the normalized coverage of ASC recordings in MLT is fairly symmetric around 2400 MLT. Further away from midnight the coverage is better in the morning than in the evening hours. Figure 4 shows the number of spiral events in each MLT bin (solid line) and the same values divided by the normalized operation hours from Figure 3 (dotted line). The normalization of the MLT distribution by the ASC operation hours does not cause significant changes.

The MLT distributions of the wintertime cloud cover at two stations, MUO and LYR, are presented in Figures 5 and 6, respectively. The amount of total cloudiness is characterised by an index varying from 0 (clear) to 8 (overcast) and 9 (impossibility of cloud observation because of rain or fog). This index value is determined once in three hours (0000, 0300, 0600 UT, etc., at MUO and 0100, 0400, 0700 UT, etc., at LYR). The histograms in Figures 5 and 6 show the occurrence of the index values larger than or equal to 4 (at least half-a-sky overcast) at the observation time (UT converted to MLT). The variation of the cloudiness is larger at MUO than at LYR. At both stations the midnight hours tend to be somewhat clearer than the evening and morning sector. At MUO the symmetry between premidnight and postmidnight is clearer than that at LYR. The cloudiness at MUO also represents well the cloudiness at the other mainland stations. The number of overcast observations (index values 8 or 9) was also very homogeneous around the midnight, while there were somewhat more clear skies observed in the postmidnight than in the premidnight sector. Thus we can conclude that the MLT distribution of spirals in Figure 2 is not significantly biased by the variation of the cloudiness.

3.2. Diameters and Wavelengths

The diameters of the spirals were measured from the images where the structure was clearest. When defining the dimensions, the structure was assumed to be located at the altitude of 110 km. In cases of elliptical spirals, we used the minor axis as a diameter.

The diameter distribution of the spirals in Figure 7 has a clear peak at values 25–75 km. All the diameters lay between 15 and 330 km. The size of the ASC field of view prohibits us from observing spirals with diam-

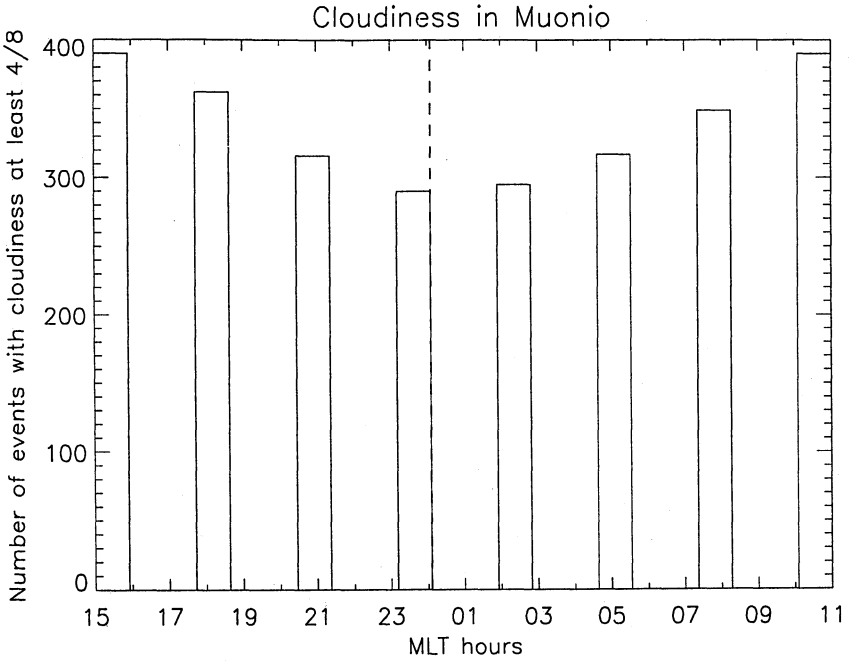

Figure 5. MLT distribution of the cloudiness in MUO during winter 1996–1997 and 1997–1998. The histogram shows the number of events when the total cloudiness has been at least 4/8. The vertical dashed line marks local magnetic midnight.

eters much larger than 300 km. The lower limit cutoff at 15 km is larger than the spatial resolution of an ASC and thus cannot be an instrumental effect. As a reference, Figure 7 also shows a diameter distribution observed by *Davis and Hallinan* [1976] (diamonds). Their results also show a cutoff but at diameters of 20 km. Their histogram is more widely spread, but it peaks at the same values as ours. A spiral population with diameters of less than 20 km (10 events) exists in our data set only, while the data set of Davis and Hallinan includes structures that are too large to be observed by the ASCs.

In our data set, there are 13 events of street spirals, 12 pairs of spirals, and one street with three spirals. The

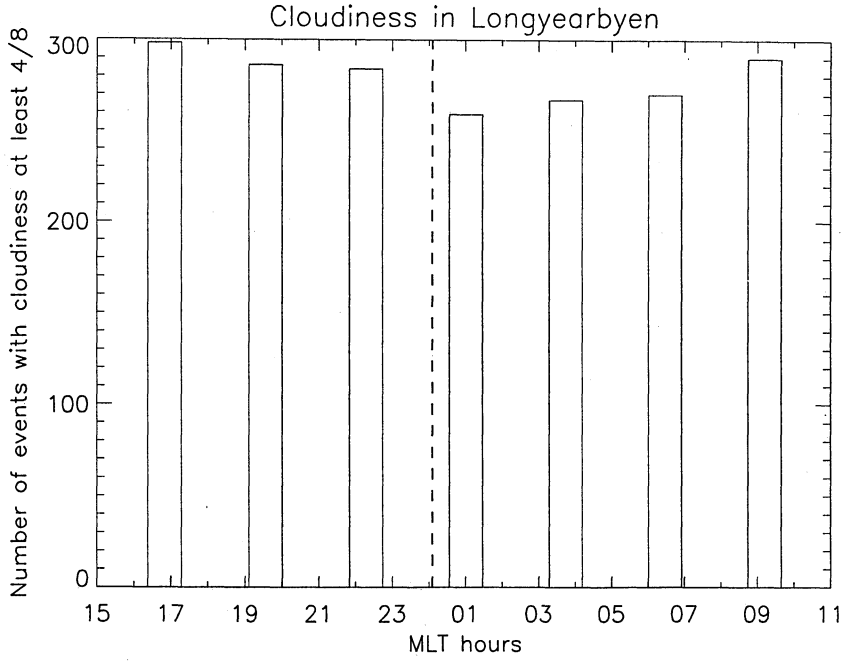

Figure 6. MLT distribution of the cloudiness in LYR during winter 1996–1997 and 1997–1998. The histogram shows the number of events when the total cloudiness has been at least 4/8. The vertical dashed line marks local magnetic midnight.

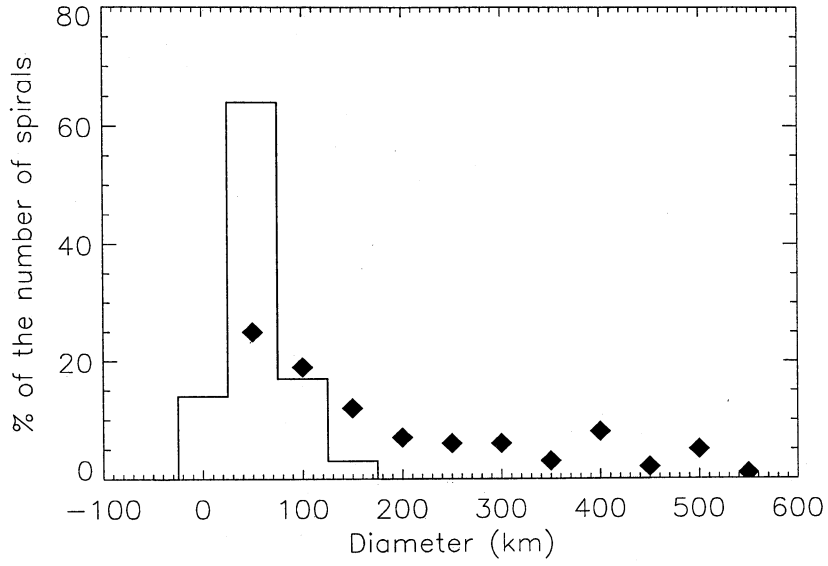

Figure 7. Diameter distribution according to our data set (histogram) with the corresponding results of *Davis and Hallinan* [1976] (diamonds after their Figure 4). The bin size is 50 km in both distributions. The first bin in our data set extends from 0 (-25) to 25 km and from 25 to 75 km in measurements by Davis and Hallinan.

sizes of the spirals in most of the streets are different. The distribution of the wavelength-diameter ratio λ/D is shown in Figure 8. It has two local maxima at 2 and 6. In two cases (7.4%) the ratio is 12, which is due to the small diameter (about 20 km) of the spirals. The size of the ASC field of view and the smallest observed diameter set an ultimate upper limit for the λ/D ratio, which is 20 (about 300 km/15 km). Again, the corresponding distribution by *Davis and Hallinan* [1976] is shown as a reference (diamonds). The two distributions cover approximately the same range, but the one by Davis and Hallinan has only one maximum at the value of 4. Furthermore, in ASC images two (or more) spirals cannot be seen at the same time unless the wavelength is very small. This means smaller λ/D ratios in the ASC observations than in the satellite images, if the diameters are assumed to be of the same order of magnitude in both data sets. One reason for this controversy can

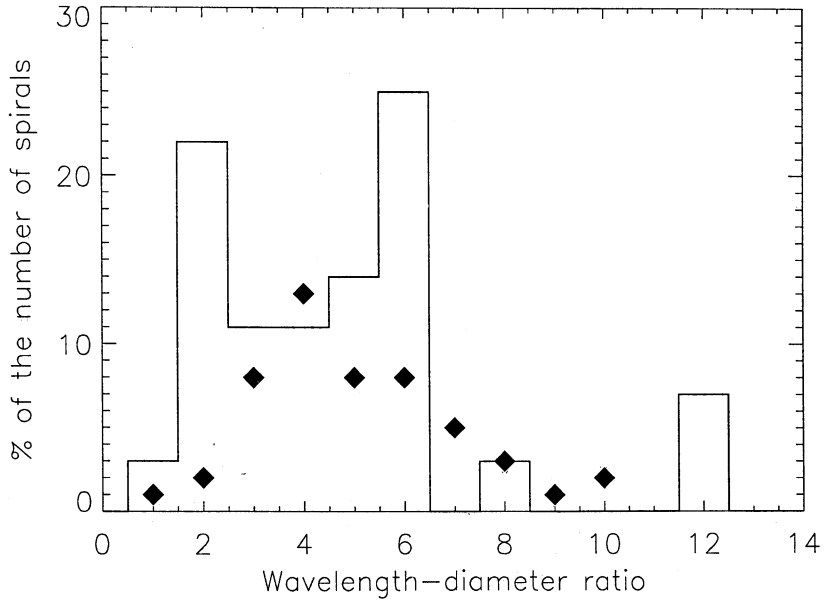

Figure 8. Comparison of λ/D ratios according to our data set to the observations by *Davis and Hallinan* [1976] (diamonds after their Figure 6).The bin size is 1.

Figure 9. Example of a westward drifting spiral. The time difference between the images is 20 s.

simply be the difference in the analysis method: while we measured the λ/D ratios for each spiral separately, Davis and Hallinan average them over one street.

3.3. Drift

We divided the spirals into four groups according to their motion: eastward and westward drifting spirals, spirals with no motion, and an indeterminate group. The few north-south drifting spirals were included with the group of no motion. The group of indeterminate motion contains the spirals that were seen only in one image, spent at most 40 s in the ASC field of view. The results showed that about 30% of the spirals do not move in the east-west direction. Furthermore, there were more eastward drifting than westward drifting events. Studying the evening and morning sides separately revealed that most of the 111 spirals observed in the morning sector (between 0000 MLT and 1200 MLT) moved eastward, and the 78 spirals in the evening sector (1200 MLT to 2400 MLT) drifted predominantly westward.

We selected 10 spirals (one from ABK, two from KEV, three from MUO, and four from KIL) that stayed in the camera field of view long enough to estimate the drift speed of the structures. The selected spirals had diameters from about 30 km to 275 km, which is approximately the same range as that for all the spirals. The drift speed was defined to be the average of the speed values calculated from the consecutive images. The 10 samples yield a range of speed values from 1 to 6 km/s, with the average value of 4 km/s. Figure 9 shows as an example of a spiral (diameter of $\approx$160 km observed at KIL on March 1, 1998) with westward speed of about 4 km/s. In this case, the speed was defined by following the eastern edge of the spiral structure.

3.4. Relation Between Spirals and Magnetic Activity

On the basis of the local B_x variations (1-min average values recorded at the ASC stations) the spirals were divided into three groups: onset spirals, which occur at the abrupt drop of B_x; expansion phase spirals, which

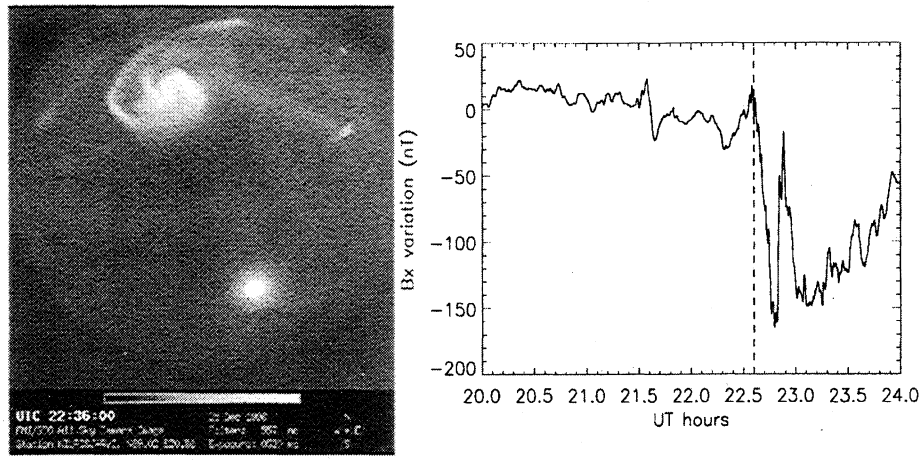

Figure 10. ASC image showing (left) an onset spiral and (right) the variation of the local B_x component on December 25, 1996, at KIL. The vertical dashed line marks the time when the ASC image was taken, 2236 UT.

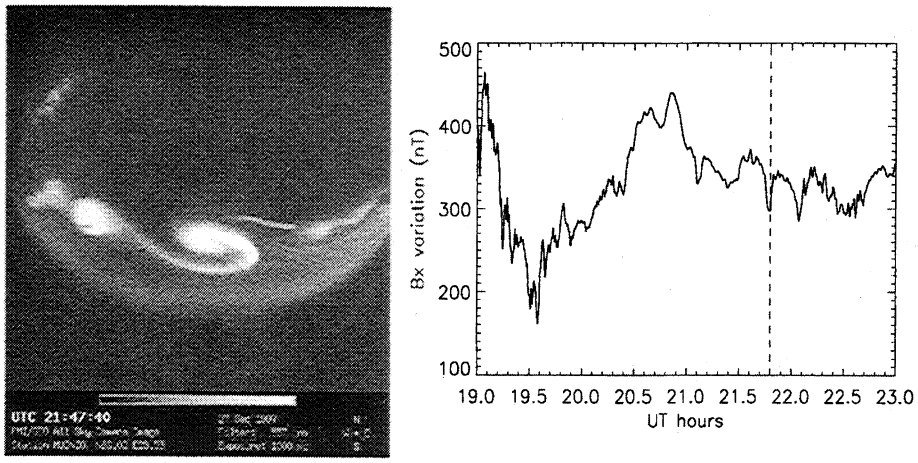

Figure 11. ASC image showing (left) a street of two spirals related with weak magnetic fluctuations ($\Delta B_x < 200$ nT) and (right) B_x variation on September 27, 1997, at MUO. The vertical dashed line marks the time when the ASC image was taken, 2147:40 UT.

occur during a negative bay of B_x; and nonsubstorm spirals, which are accompanied with magnetic variations smaller than 200 nT. Figures 10 and 11 show an example of an onset spiral and a quiet time spiral, respectively; 61% of our spirals are nonsubstorm spirals, 27% are expansion phase spirals, and 12% are onset spirals (see Figure 12). Neither diameter nor wavelength values indicated correlation with these three local substorm phases.

The 23 onset-associated spirals took place around the local magnetic midnight, 2100–0300 MLT. With the available instrumentation it is very difficult to determine whether these local onsets are precursors of the global substorm activity. Polar UV images, which show the global distribution of the auroras and have time resolution high enough, were available for only a few events. In order to get a better view on the global activity, we examined the data of the Greenland magnetometer chains, which are roughly 40° and 90° east of the IMAGE magnetometers, and the particle flux data of the Los Alamos National Laboratory (LANL) instruments on board geostationary satellites. In most of the cases (18 out of 23) the IMAGE magnetometers recorded the onset earlier than Greenland magnetometers or any of the LANL satellites. Thus IMAGE was predominantly close to the global onset region. In cases when IMAGE saw the onset later than Greenland or LANL, the time difference was $\leq$6 min. Without ex-

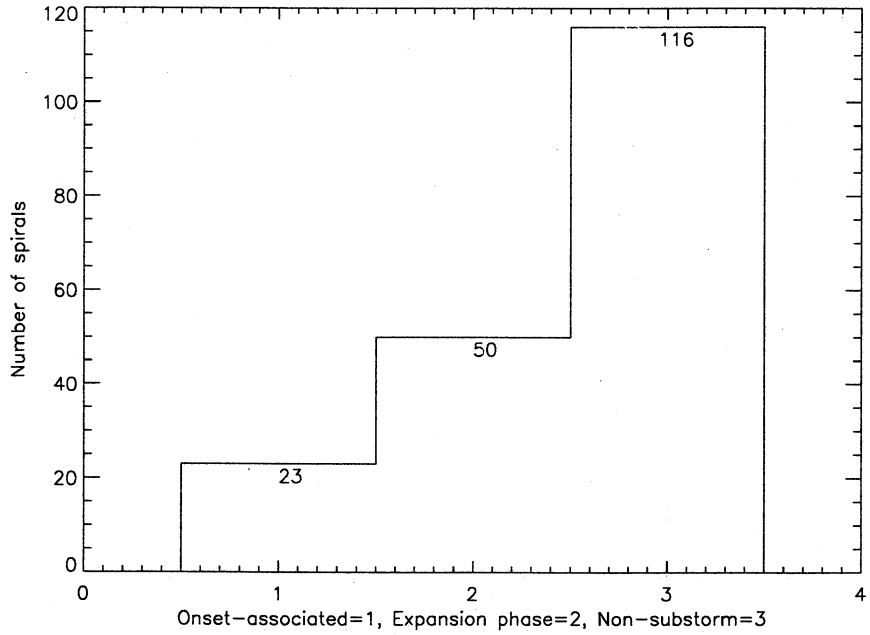

Figure 12. Distribution of substorm phases related to spirals: onset-associated spirals, expansion phase spirals, and nonsubstorm spirals (for definitions, see text).

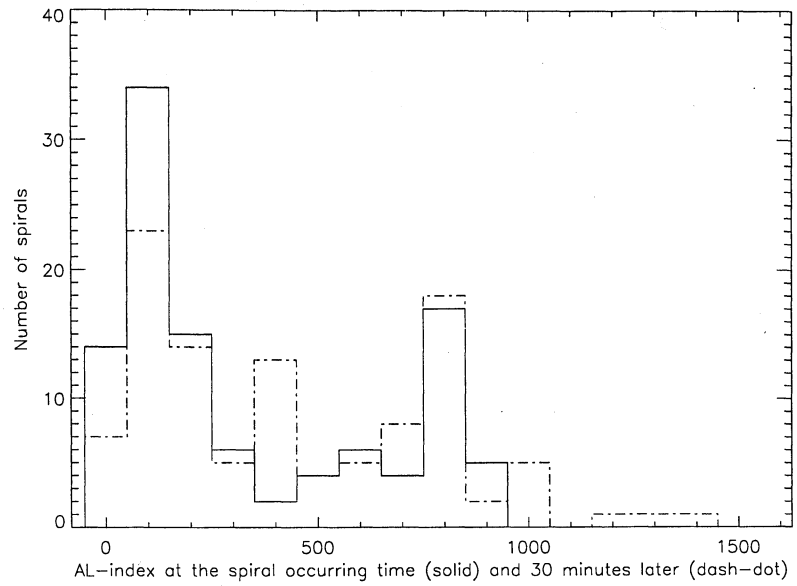

Figure 13. Distributions of IL_0 (solid line) and IL_{30} (dash-dot line). (For definitions of IL_0 and IL_{30}, see text.)

ception, the onset spirals appeared at the onset time or later. We observed no spirals appearing immediately before the onset.

We created a reference data set of both ΔB_x values and local substorm phases (quiet time, expansion phase, and onset) recorded 24 hours after the spiral occurrence time. This was done in order to see whether the distribution of these parameters for spirals is different from the corresponding randomly collected data set. The reference distribution of the ΔB_x intensity appeared to be very similar to that of the spirals, which means that the spirals do not necessarily cause strong magnetic variations. The random phase distribution (95% quiet time, 4% expansion phase, 1% onset) is different from the spiral phase distribution (61% quiet time, 27% expansion phase, 12% onset; see Figure 12), which in turn shows that although most of the spirals tend to occur during magnetically quiet time, there is also a group of westward traveling surge (WTS) type spirals appearing under disturbed conditions.

The *IL* index calculated from the IMAGE magnetometer network gives a good estimate of global *AL* index during 2100–0200 UT [*Kauristie et al.*, 1996]; 57% of the 189 spiral events took place in this UT range. In the following, we limit our analysis to this smaller data set. In order to further investigate the role of the spirals as triggers of substorm activity, we studied the absolute values of *IL* (hereinafter called just *IL*) at three moments: at the time of the spiral occurrence (IL_0), 15 min later (IL_{15}), and half an hour later (IL_{30}). Also, the maximum *IL* of the next half an hour period ($IL_{\max}$) was used in the analysis. If the magnetic activity systematically increased after the spiral occurrence time, the peak value of IL_0 distribution would be at a smaller value than that of IL_{15} or IL_{30}. However, both the IL_0 and IL_{30} distributions peak at the same value (Figure 13). The IL_{30} distribution is somewhat wider, which is most probably due to the subgroup of WTS-type spirals.

We also defined IL_{30} distributions separately for three groups for spirals with $IL_0 < 200$ nT, 200 nT $< IL_0 <$ 600 nT, and $IL_0 > 600$ nT. Results are shown in Figure 14. The *IL* values of the first group ($IL_0 < 200$ nT) have spread somewhat to larger values after 30 min, but the clear peak of IL_{30} remains at the same place as that of IL_0. This indicates that most of these spirals are really quiet time structures and not precursors of increasing magnetic activity. In the second group, both IL_0 and IL_{30} distributions are flat and do not reveal any coherent behavior. The peak value of the third group remains around the same *IL* range after 30 min, which suggests that these spirals were observed during longer periods ($\geq$0.5 hour) of high activity. An interesting detail is that the spirals which occur only in one ASC image (drift or fade away before the next image is taken) can be associated with increasing activity. The distribution of $IL_{\max}$ (not shown) for such events has maximum at ~1000 nT, while $IL_{\max}$ of the other events is typically around 300 nT.

Figure 15 shows a different way of putting the *IL* discussion above. We still considered the three groups defined by IL_0. For each group separately we plotted the difference $IL_{30} - IL_0$ as a function of MLT. No matter what the initial *IL* value is, the activity increases in most of the cases ($IL_{30} - IL_0 > 0$). However, the differences show no systematic behavior according to MLT. Thus the spirals related with increasing activity do not have a tendency to favor any certain MLT sector.

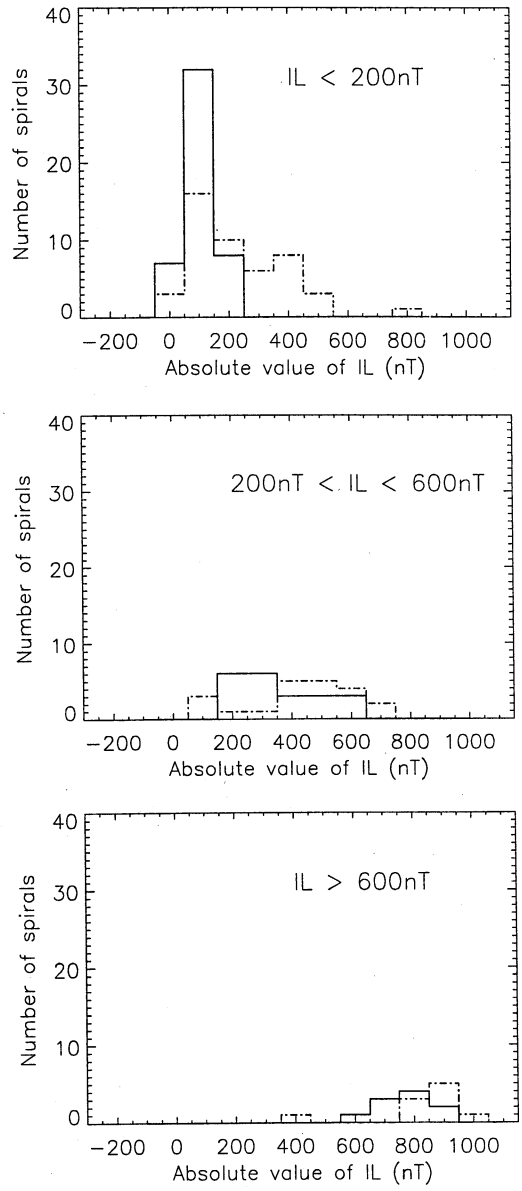

Figure 14. Distributions of IL_0 (solid line, IL in the figure) and IL_{30} (dashed lines) (for definitions, see text): (top) $IL_0 < 200$ nT, (middle) 200 nT $< IL_0 <$ 600 nT, and (bottom) $IL_0 > 600$ nT.

4. Comparisons With Previous Studies and Discussion

Our statistics show clearly that the majority of the spirals occur during magnetically quiet conditions. This does not agree with previous studies which relate spirals with disturbed periods [*Davis and Hallinan*, 1976; *Samson et al.*, 1996]. Davis and Hallinan found most of the spirals from global-scale images acquired by the cameras of DMSP satellites during the expansion and early recovery phases of substorms. The disagreement is at least partly due to differences in the definition of quiet time. We used magnetic field data, while Davis and Hallinan deduced the activity level and substorm phase from the global auroral images. However, in our data set quiet time spirals also dominate when IMAGE is in the magnetic midnight sector, i.e., in the region where the strongest activity most probably takes place.

In the DMSP data set of Davis and Hallinan, spirals appear most frequently in the evening and the midnight sector (MLT), while our ASC recordings, which have a better MLT coverage than the satellite images, show more spirals in the postmidnight sectors. In the late morning sector (between 0400 and 0800 MLT), *Davis and Hallinan* [1976] observed quiet time spirals (satellite images) and small transient spirals during very active conditions (ASC data). We did not find any correlation between the size of the spirals and the level of magnetic activity in the morning sector, but the relative contribution of disturbed time spirals is larger between 0400

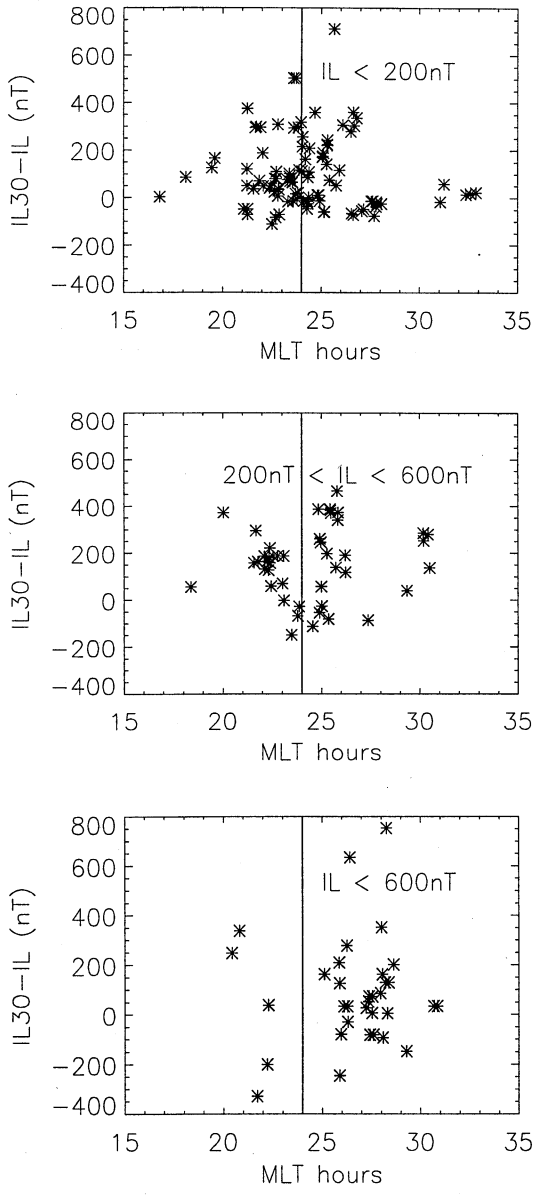

Figure 15. Difference between IL_{30} and IL_0 (IL in the figure) as a function of MLT: (top) $IL_0 < 200$ nT, (middle) 200 nT $< IL_0 <$ 600 nT, and (bottom) $IL_0 >$ 600 nT. The vertical lines mark magnetic midnight.

and 0800 MLT than in the other MLT sectors. This finding suggests that the group of small and transient spirals dominates our ASC data set.

Hallinan [1976] presented a theoretical model to explain the spiral formation as a consequence of Kelvin-Helmholtz instability. According to this model, an enhanced current filament within an upward directed field-aligned current sheet (an auroral arc) causes bending of the field lines. A small distortion at the magnetospheric end of the field lines grows earthward and forms a completely wound spiral at the ionospheric end of the system. This model predicts a certain preference range (16–20) for the ratio between the wavelength and the arc width ($\lambda/2a$). Davis and Hallinan defined these ratios for 18 events and obtained values consistent with the model predictions. Furthermore, for a larger data set they achieved a typical value of 4 for the ratio λ/D. Consequently, our similar results of λ/D (typically 2–6) can be considered as an indirect support to the spiral model by Hallinan.

Vortex formation due to an unstable growth of field line resonance (FLR) has been discussed by *Samson et al.* [1996] and *Voronkov et al.* [1999]. Samson et al. relate some of the large spirals within discrete arcs with FLR and triggering of the substorm onset. This should appear as a correlation between the occurrence of large spirals and an increase in magnetic activity (*IL* index), but our data set does not show such correlation. However, the fastest spirals (appearing in one ASC image only) were followed by increasing *IL* values within the next 30 min. Either the FLR-related spirals may be spatially too large for ASC observations, or their winding may not be complete enough to fulfill our selection criterion.

When browsing ASC images only, spirals can be confused with westward traveling surges or omega bands. A WTS may look very much like a spiral, as its western edge winds in the same sense as spirals do. Similarly, the auroral tongues in the omega bands may develop into spiral-like structures. Although WTS and omega bands look similar to spirals, they have clear associations with substorm phases (WTSs occur during expansion phase, and omega bands occur during recovery phase [*Opgenoorth et al.*, 1994]), while the connection between spirals and substorms is not so clear.

Evening sector spirals move preferentially westward, and morning sector spirals move eastward. Thus the spiral motion follows the large-scale convection. In addition, fast spirals (occurring in one ASC image only) are related to increasing *IL* values, which implies enhanced convection. It is interesting to compare our result of a spiral mean velocity of 4 km/s with the speeds of the other similar auroral structures: folds and curls have speeds of at most 5 km/s and 90 km/s, respectively [*Davis and Hallinan,* 1970; *Trondsen and Cogger,* 1998], drift velocity of omega bands is typically below 1.5 km/s and speeds of AAFs are 1–2 km/s [*Elphinstone et al.*, 1996]. Fine-scale structures (rays) within arcs have velocities of up to 20 km/s [*Lanchester and Rees,* 1987]. The westward traveling surge moves typically with a speed of a few kilometers per second, and an auroral horn (brightening of a pre-existing arc) has a speed of 10–30 km/s [*Koskinen et al.*, 1990]. Thus spirals drift slower than curls and horns and with about the same speed as folds, surges, and omegas do. Spirals are larger than curls but are usually of the same size as folds. Hence the speed of an auroral structure seems to anticorrelate with its size.

5. Summary and Conclusions

The auroral spiral forms observed by the ASCs of the MIRACLE network [*Syrjäsuo et al.*, 1998] during winters 1996-1997 and 1997-1998 were analyzed statistically. The analysis reproduced some of the previously published results based on satellite and all-sky camera observations, now with a new aspect of better temporal and spatial resolution of the new ASCs. The typical spiral diameter (D), the wavelength (λ, distance between adjacent spirals), and the ratio between the wavelength and the diameter found in this study ($D \sim$ 25–75 km, $\lambda \sim$ 125–175 km, and $\lambda/D \sim$ 2–6) agrees with the corresponding parameters obtained by *Davis and Hallinan* [1976]. On the other hand, our ASCs recorded more spirals in the morning than in the evening MLT hours, while the data set of Davis and Hallinan was dominated by premidnight sector spirals.

A new aspect of this work is the systematic comparison of the ASC and magnetic data. Magnetic recordings at the ASC stations were used to characterize the local activity level, and the *IL* index derived from the data of the whole IMAGE network was utilized to estimate the larger-scale activity. Such analysis revealed that spirals appear during both weak ($IL \sim$ 100 nT) and strong ($IL \sim$ 800 nT) magnetic activity. Contrary to previously published studies, our statistical analysis shows that a major part of the spirals occur during magnetically quiet conditions which persist at least half an hour after the spiral observation. However, fast-moving spirals, which occur only in one ASC image, seemed to be related to increasing activity within the next 30 min. The active time spirals occur during extended periods of activity. We did not find any significant correlation between the size of the spirals and magnetic activity.

Acknowledgments. The work by N.P. was supported by the Finnish Graduate School in Space Physics and Astronomy. We thank Jürgen Watermann from the Danish Meteorological Institute for providing us with the Greenland magnetometer data, George Reeves for the Los Alamos National Laboratory satellite data, and the Climatology Division of the Norwegian Meteorological Institute for the Longyearbyen cloud data. The MIRACLE network is operated as an international collaboration under the leadership of the Finnish Meteorological Institute. The IMAGE magnetometer data are collected as a Finnish-German-Norwegian-Polish-Russian-Swedish project.

Michel Blanc thanks Asgeir Brekke and another referee for their assistance in evaluating this paper.

References

Davis, T. N., and T. J. Hallinan, Small-scale auroral arc distortions, *Planet. Space Sci., 18,* 1735-1744, 1970.

Davis, T. N., and T. J. Hallinan, Auroral spirals, 1., Observations, *J. Geophys. Res., 81,* 3953–3958, 1976.

Elphinstone, R. D., J. S. Murphee, and L. L. Cogger, What is a global auroral substorm?, *Rev. Geophys., 34,* 169–232, 1996.

Hallinan, T. J., Auroral spirals, 2., Theory, *J. Geophys. Res., 81,* 3959–3965, 1976.

Kauristie, K., T. I. Pulkkinen, R. J. Pellinen, and H. J. Opgenoorth, What can we tell about global auroral-electrojet activity from a single meridional magnetometer chain?, *Ann. Geophys. Lett., 14,* 1177–1185, 1996.

Koskinen, H. E. J., T. I. Pulkkinen, and R. J. Pellinen, Mapping of the auroral horn into the magnetotail, *Planet. Space Sci., 38,* 1179–1186, 1990.

Lanchester, B. S., and M. H. Rees, Field-aligned current reversals and fine structure in a dayside auroral arc, *Planet. Space Sci., 35,* 759–768, 1987.

Opgenoorth, H. J., M. A. L. Persson, T. I. Pulkkinen, and R. J. Pellinen, *J. Geophys. Res., 99,* 4115–4129, 1994.

Samson, J. C., L. L. Cogger, and Q. Pao, Observations of field line resonances, auroral arcs, and auroral vortex structures, *J. Geophys. Res., 101,* 17,373–17,383, 1996.

Syrjäsuo, M. T., et al., Observations of substorm electrodynamics using the MIRACLE network, *Proc. Int. Conf. Substorms 4th, 238,* 111–114, 1998.

Trondsen, T. S., and L. L. Cogger, A survey of small-scale spatially periodic distortions of auroral forms, *J. Geophys. Res., 103,* 9405–9415, 1998.

Voronkov, I., R. Rankin, J. C. Samson, and V. T. Tikhonchuk, Shear flow instability in the dipolar magnetosphere, *J. Geophys. Res., 104,* 17,323–17,334, 1999.

M. Brittnacher, Geophysics Program, Box 351650, University of Washington, Seattle, WA 98195. (britt@geophys.washington.edu)

K. Kauristie, N. Partamies, and T. I. Pulkkinen, Finnish Meteorological Institute, Geophysical Research, P.O. Box 503, FIN-00101 Helsinki, Finland. (kirsti.kauristie@fmi.fi; noora.partamies@fmi.fi; tuija.pulkkinen@fmi.fi)

(Received July 7, 2000; revised October 27, 2000; accepted December 6, 2000.)